Materials for Renewable and Sustainable Energy (2019) 8:1
https://doi.org/10.1007/s40243-018-0138-4

ORIGINAL PAPER

Electrochemical properties of chemically synthesized SnO_2-RuO_2 mixed films

S. N. Pusawale[1,2] · P. R. Deshmukh[2] · P. S. Jadhav[1] · C. D. Lokhande[2,3]

Received: 4 May 2018 / Accepted: 30 October 2018 / Published online: 10 November 2018

Abstract

The SnO_2–RuO_2 mixed films are prepared by successive ionic layer adsorption and reaction (SILAR) method. The SnO_2 films combined with RuO_2 are prepared by varying the deposition cycles of SILAR. The effect of combining SnO_2 with RuO_2 on structural, morphological and electrochemical properties is studied. It is observed that the crystalline nature of SnO_2 changed to amorphous with increase in RuO_2 deposition cycles. The morphology is also changed from fibrous-porous to compact after increasing RuO_2 deposition cycles. The specific capacitance of SnO_2 is increased from 4 to 185 F/g after combined with RuO_2. The maximum utilization of RuO_2 is observed with specific capacitance of 1010 F/g.

Keywords Chemical synthesis · SnO_2, RuO_2 · Thin films · Supercapacitor · Charge–discharge

Introduction

Electrochemical capacitors or supercapacitors have the considerable attraction in recent years due to the growing demand of power sources. Supercapacitors have the wide range of applications in various areas such as hybrid electric vehicles, telecommunications, particularly associated with cellular phones for a reduction of the size of the batteries [1], memory protection of computer electronics [2, 3], etc. Supercapacitors are divided into two categories according to the principles involved in energy storage, namely [4] (1) electric double layer capacitor (EDLC) and (2) pseudocapacitor. The energy in EDLC is stored across the double layer formed at the interface between an electrode and the electrolyte, while in the case of pseudocapacitor it is based upon the reversible Faradaic reactions taking place at the interface between the electrode and electrolyte in an appropriate potential range. The EDLC's are based on carbon materials with high surface area, while pseudocapacitors are based on metal oxides and conducting polymers.

Recently extensive research is focused on the supercapacitor behavior of metal oxide electrodes. Among the various metal oxides, the hydrous form of RuO_2 has shown excellent supercapacitive behavior. The high specific capacitance is attributed to proton intercalation into the bulk material of hydrous RuO_2 [5–8].

Although RuO_2 is more promising material for supercapacitors, it has the disadvantage of very high cost and toxic nature, which limits its commercial use. Therefore, several studies are going on combining RuO_2 with other materials such as VO_x, TiO_2, NiO, WO_3, SnO_2, etc., to minimize the use of Ru precursors and hence to decrease the cost of the precious metal. It is observed that addition of SnO_2 in RuO_2 matrix increases the utilization of Ru species and enhance the electrochemical stability. Moreover, SnO_2 has same rutile structure as RuO_2 with lattice parameters of both quite similar to each other (SnO_2, $a=b=4.7382$ Å and $c=3.1871$ Å; RuO_2, $a=b=4.4994$ Å and $c=3.1071$ Å) [9]. Hu et al. used the modified sol–gel process for deposition of ruthenium–tin oxide composites with a maximum specific capacitance of 690 F/g [10]. Kim et al. used a DC reactive sputtering method for the preparation of the composite RuO_2–SnO_2 electrode which showed a maximum specific capacitance of 88.8 F/g [11]. Wang and Hu adopted a mild hydrothermal process to synthesize hydrous ruthenium oxide-tin oxide composites ((Ru–Sn)O_2 nH_2O where a maximum specific

✉ C. D. Lokhande
l_chandrakant@yahoo.com

[1] Rajarambapu Institute of Technology, Rajaramnagar (Sakharale), Islampur 415409, Maharashtra, India

[2] Thin film Physics Laboratory, Department of Physics, Shivaji University, Kolhapur 416004, Maharashtra, India

[3] D. Y. Patil University, Kolhapur 416006, Maharashtra, India

capacitance is 830 F/g [12]. A composite tin oxide-ruthenium oxide supercapacitor electrode synthesized by cyclic voltammetric plating of RuO_2 onto a porous and highly conductive SnO_2 showed a specific capacitance of 930 F/g [13]. A specific capacitance of 150 F/g was observed for SnO_2–RuO_2 composite thin films prepared by chemical bath deposition [14].

In the present study we have adopted successive ionic layer adsorption and reaction (SILAR) method which has various merits such as a low-temperature synthesis for deposition of metal oxides, simple and inexpensive, excellent material utilization efficiency, good control over deposition process along with film thickness, etc. [15]. In the present investigation, we report on the synthesis of SnO_2-RuO_2 mixed films by SILAR method and its electrochemical properties.

Materials and methods

Preparation of SnO_2–RuO_2 mixed films

The SnO_2–RuO_2 mixed thin films are deposited on stainless substrates by SILAR method using the 5-beakers system. The schematic experimental setup for deposition is shown in Fig. 1a.

The cationic solutions of 0.05 M stannous chloride ($SnCl_2{\cdot}2H_2O$) and 0.01 M ruthenium chloride ($RuCl_3{\cdot}xH_2O$) are taken in separate beakers as sources of tin (Sn^{4+}) and ruthenium (Ru^{3+}) ions, respectively. The anionic solutions consist of 1% H_2O_2 and hot water maintained at 343 K as sources of oxygen and OH^- ion, respectively. To vary the content of SnO_2 and RuO_2 in the mixed film, the cycle ratio of SnO_2:RuO_2 deposition is varied. The SnO_2-RuO_2 mixed films of 3:2, 1:1, 1:3 and 2:3 cycle ratios are named as S1, S2, S3 and S4 and used in further studies. Figure 1 b shows the photograph of SnO_2-RuO_2mixed films on stainless steel substrates (> 8 cm^2 area). The thickness of the films is in the range between 0.5 and 1 μm.

Characterization techniques

X-ray diffraction patterns are obtained using a Philips (PW-3710) diffractometer with a Cr Kα ($\lambda = 2.2870$ Å) target, to study the structural property of films, The FT-Raman spectrograms are obtained using Bruker make Raman spectrophotometer. The microstructure of the films is observed using field emission scanning electron microscopy (FE-SEM) (JSM 7100F). The electrochemical study is performed in a three-electrode configuration cell consisting of the SnO_2–RuO_2 mixed film as a working electrode, platinum as a counter electrode and saturated calomel electrode (SCE) as a reference electrode. The charge–discharge analysis is performed by WonATech Automatic Battery Cycler WBCS system, interfaced to a computer. The electrochemical impedance measurements are conducted with a versastat 3G frequency response analyzer (FRA) under Zplot program (Scribner Associates Inc.)

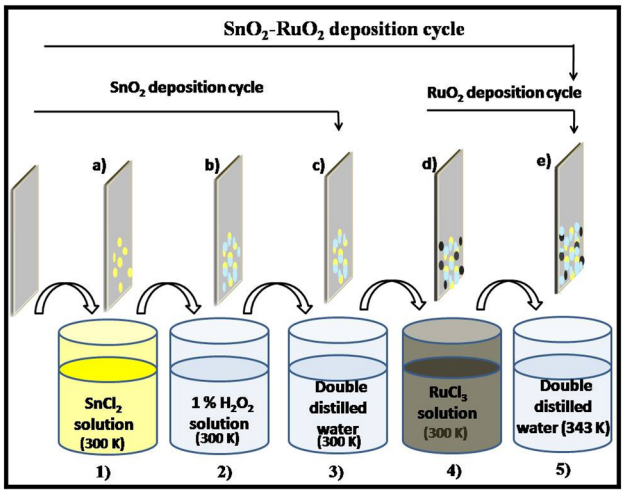

(a)

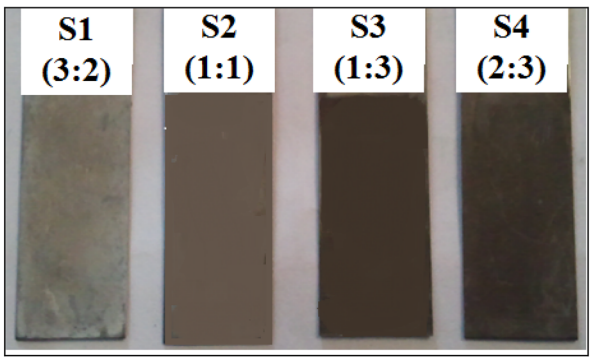

(b)

Fig. 1 **a** Schematic experimental setup of SILAR method for deposition of SnO_2–RuO_2 mixed film, **b** Photograph of SnO_2–RuO_2 mixed films deposited by SILAR on stainless steel substrate (> 8 cm^2 area)

Result

Reaction mechanism of SnO_2–RuO_2 mixed thin film formation

The general reaction mechanism for SnO_2–RuO_2 mixed film formation by SILAR method can be described as follows: First 0.05 M $SnCl_2.2H_2O$ is dissolved in concentrated hydrochloric acid, and the mixture kept for heating at 363 K for 5 min. The reaction proceeds as

$$SnCl_2 \cdot 2H_2O + 2HCl \xrightarrow{\Delta} SnCl_4 + 2H_2O + 2H^+ \quad (1)$$

In aqueous acidic solution, Sn^{4+} ions hydrolyze to form highly insoluble stannic hydroxide ($Sn(OH)_4$) which precipitates on the substrate surface immersed in it.

$$Sn^{4+} + 4H_2O \rightarrow Sn(OH)_4 + 4H^+ \quad (2)$$

The substrate covered with $Sn(OH)_4$ is rinsed in dilute H_2O_2 solution, where the formation of SnO_2 takes place as

$$Sn(OH)_4 + H_2O_2 \rightarrow SnO_2 + 3H_2O + \frac{1}{2}O_2 \uparrow \quad (3)$$

The substrate coated with SnO_2 is then cleaned in double-distilled water to remove loosely bound particles and excess H_2O_2 from the substrate surface. It is observed that if this step is not followed, then excess H_2O_2 on the substrate surface reacts with $RuCl_3$ solution and precipitation of ruthenium hydroxide ($Ru(OH)_3$) is observed in $RuCl_3$ solution without RuO_2 film formation. Therefore, it is necessary to rinse the substrate in double-distilled water after SnO_2 film formation.

The mechanism for RuO_2 film formation is same as described by Patake and Lokhande [16]. The substrate coated with SnO_2 is immersed in the $RuCl_3$ solution, where the Ru^{3+} ions are adsorbed on the substrate surface. The substrate with adsorbed Ru^{3+} ions is immersed in hot water bath (343 K) where OH^- ions react with Ru^{3+} ions to form $Ru(OH)_3$ through the reaction

$$Ru^{3+} + 3OH^- \rightarrow Ru(OH)_3 \quad (4)$$

The excess OH^- ions then react with $Ru(OH)_3$ to form RuO_2 as

$$Ru(OH)_3 + OH^- \rightarrow RuO_2 + 2H_2O \quad (5)$$

This completes the one cycle for the SnO_2–RuO_2 mixed film formation. The mixed films of various cycle ratios are prepared by keeping the total number of cycles constant.

As the method employed in this work is low-temperature synthesis method with deposition directly from solution in the form of thin film, it is somewhat difficult to predict how much SnO_2 and RuO_2 will be involved in the deposition process like other chemical methods wherein weighed amount of elements is mixed into each other to form required composite. The techniques like EDAX will only give an idea about elements present but not the weight fraction. The XRD curves are also not useful as one of the phase RuO_2 is in the amorphous form. Due to unavailability of other techniques, in this work we have adopted a simple method to estimate the mass of SnO_2, RuO_2 and mass fraction in the mixed films. Each sample has certain cycles of SnO_2 and RuO_2 depositions. First we measured the mass of bare substrate and on it SnO_2 deposition is carried out as per given cycle ratio. The substrate coated with SnO_2 is weighed thereafter. This gives the approximate estimation of how much SnO_2 is deposited in the one cycle; thereafter, same procedure is followed with RuO_2 to get an idea about how much mass of RuO_2 is deposited during one cycle. After the required number of cycles for given sample the total mass of the sample is measured. Using this total mass of mixed films and total number of deposition cycles of only SnO_2/RuO_2 the approximate mass of SnO_2/RuO_2 in the mixed film is calculated. The total mass of mixed films and mass fraction of SnO_2 and RuO_2 are given in Table 1.

Table 1 Mass and mass fraction of SnO_2-RuO_2 mixed films for different cycle ratio

Sample	S1 (3:2)	S2 (1:1)	S3 (1:3)	S4 (2:3)
Mass of mixed film (gm)	0.01213	0.0061	0.00279	0.0011
Mass fraction of RuO_2	0.1515	0.1532	0.1792	0.1979
Mass fraction of SnO_2	0.8485	0.8541	0.8208	0.8021

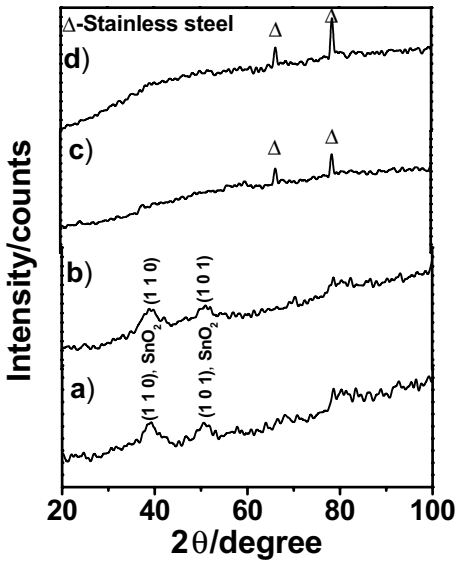

Fig. 2 The X-ray diffraction patterns of SnO_2–RuO_2 mixed films for samples **a** S1 (SnO_2:RuO_2, 3:2), **b** S2 (1:1), **c** S3 (3:1) and **d** S4 (2:3)

Structural analysis

The X-ray diffraction patterns of SnO_2–RuO_2 mixed films with various cycle ratios are presented in Fig. 2. The XRD pattern of sample S1 is shown in Fig. 2a), from which the broad diffraction peaks are observed at the $2\theta = 39.06°$ and 50.92° which corresponds to the cassiterite SnO_2 for (1 1 0) and (1 0 1) planes, respectively (JCPDS card no. 77-0452). No diffraction peaks for RuO_2 are observed, which might be due to the formation of amorphous RuO_2. The formation of amorphous RuO_2 is mainly observed in the low-temperature chemical synthesis [16, 17]. For the sample S2, the XRD pattern in Fig. 2b) showed the broader diffraction at the

above angles as compared with sample S1 that revealed the formation of oxide in nanometer scale. In the case of samples S3 and S4 no broader diffractions are observed (Fig. 2c, d) which may be due to the increased RuO_2 content in the film, which leads to the formation of the amorphous phase. The diffraction peaks observed in these two samples are due to the stainless steel substrate. Thus, the XRD studies revealed the transition from nanocrystal line to amorphous phase of mixed films with the increase in RuO_2 content in the film.

FT-Raman study

The typical Raman spectra of SnO_2, RuO_2, and SnO_2–RuO_2 mixed films are shown in Fig. 3. Figure 3a shows the Raman spectrum of SnO_2 with Raman shifts at 620 and 777 cm^{-1} corresponding to the crystallites of SnO_2 with a tetragonal rutile structure (i.e. A_{1g} and B_{2g}) [18]. The Raman shift at 564 cm^{-1} corresponds to amorphous SnO_2. The other Raman shifts observed at 248 and 324 cm^{-1} correspond to the N group vibration modes of SnO_2 nanocrystallites, which are referred to a large number of vacant lattice positions and local lattice disorders [18]. In Fig. 3b Raman shifts are observed at 526, and 640 cm^{-1} corresponding to the E_g and A_{1g} vibration modes of RuO_2 [19]. The Raman spectrum

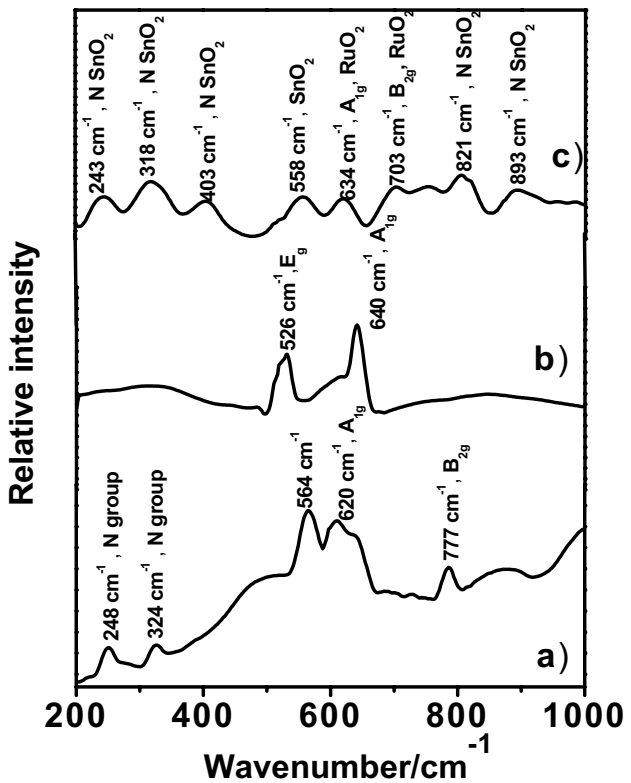

Fig. 3 FT-Raman spectra of **a** SnO_2, (b) RuO_2 and (c) SnO_2-RuO_2 mixed thin films

of the SnO_2-RuO_2 mixed film is shown in Fig. 3c. In curve c, the shifts at 634 and 703 cm^{-1} correspond to crystalline RuO_2 (i.e. A_{1g} and B_{2g}) in the rutile form, whereas as the Raman shift at 558 cm^{-1} is due to the amorphous SnO_2. In comparison with Fig. 3a, b the shift in positions in Fig. 3c for SnO_2 and RuO_2 observed is due to the quantum effects of the decrease in particle size [20]. However, the certain new shifts observed in Fig. 3c might be due to the SnO_2–RuO_2 mix state formation [21].

Surface morphological and composition studies

The effect of various cycle ratios of SnO_2–RuO_2 on the surface morphology of mixed films is studied using scanning electron microscopy. Figure 4 shows the SEM images of mixed films for various cycle ratios. From the SEM image of sample S1 (3:2) (Fig. 4a), the irregularly arranged agglomerates forming a rough surface with porous morphology is observed. The SEM image of sample S2 (1:1) is shown in Fig. 4b from which well-covered surface of the nanocrystallites is observed; further these nanocrystallites are arranged in such a way that highly porous and fibrous structure is formed. The morphology showed the decrease in the porous structure of the film compared with the morphology of sample S1. The SEM image of sample S3 (1:3) showed larger agglomerates with comparatively smooth morphology (Fig. 4c). The SEM image of sample S4 (2:3) shows the small agglomerates covered over the entire substrate surface with less porous morphology (Fig. 4d). The SEM images strongly confirm the dependence of morphology of mixed film on SnO_2–RuO_2 cycle ratio. It is observed that the mixed film with higher RuO_2 cycle (sample S3) has a smooth morphology with less porous structure. On the other hand, the film with higher SnO_2 cycle is highly porous (sample S1 and S2). It is observed that the addition of SnO_2 into RuO_2 increases the effective surface area of the net material. As confirmed by the XRD studies, the samples S1 and S2 have smaller crystallites in the nanometer range, which results in the high surface area by offering the porous morphology. Figure 4e) shows EDAX studies of mixed thin films for different cycle ratio and Table 2 gives the atomic percentage of Sn, Ru and O present in the sample. It is observed that the atomic percentage of Sn and Ru varies as a function of ratio of deposition cycles. Ru content increases with increase in deposition cycle of RuO_2.

Electrochemical studies

The typical cyclic voltammetric behavior of pure SnO_2 film prepared by SILAR method and SnO_2–RuO_2 mixed films is measured in 0.5 M H_2SO_4 electrolyte in the potential range of − 0.2 to +0.6 V vs. SCE at 5 mV/s scan rate is shown in Fig. 5a. The CV curve for pure SnO_2 shows double layer

capacitance due to the absence of redox reactions in the given potential region with negligible current response in microamperes. The observed double-layer capacitance for SnO_2 is about ~ 4 F/g that is very small and can be neglected. The increase in the current response is observed only after the introduction of RuO_2 into SnO_2. The CV curves for the mixed film shows that the characteristic of the capacitance is different from that of the electric double-layer capacitance, in which the CV curve is close to the ideal rectangular shape. From a comparison of curves (b) to (e) in Fig. 5, an obvious decrease in the voltammetric current and less symmetric I–V curves are found for more SnO_2 cycles samples. The small capacitive current measured for potentials below +0.4 V vs. SCE is commonly attributed to the high density of bound water, and OH^- formed on the surface of RuO_2 particles [22]. This water plays the role of a potential barrier for the electrons hindering the electron hopping process between the particles of the material.

The total specific capacitance (denoted as $C_{S,T}$) and the specific capacitance based on RuO_2 (denoted as $C_{S,Ru}$) can be estimated from a cyclic voltammogram according to Eqs. (6) and (7) [22–24].

$$C_{\mathrm{S,T}} = \frac{Q}{V} = \frac{\int I\mathrm{d}t}{m\Delta V} \tag{6}$$

$$C_{S,Ru=}\frac{C_{S,T} - C_{S,Sn}}{w_{Ru}}, \tag{7}$$

where $\int I\mathrm{d}t$ is the total current obtained by integrating area under the curve, m is the mass of the electrode, ΔV is the electroactive potential range for electrode, and $C_{S,T}$, $C_{S,Ru}$, $C_{S,Sn}$ and w_{Ru} are the specific capacitance of mixed film, RuO_2 species, bare SnO_2, and the weight fraction of RuO_2 within the mixed film, respectively.

The dependence of $C_{S,T}$, and $C_{S,Ru}$ on the Sn and Ru content for samples S1 to S4 is shown in Table 3. The $C_{S,T}$ of the film is increased from sample S1 to S3 with maximum value of 185 F/g after that it decreased to 81 F/g for sample S4. The $C_{S,Ru}$ value is also increased from 33 to 1010 F/g from sample S1 to S3 after which it decreased to 389 F/g for sample S4.

For sample S4, the value of $C_{S,Ru}$ is less compared with sample S3, which means utilization of RuO_2 is poor for sample S4. Thus, sample S3 is found to be a better sample for the production of SnO_2–RuO_2 mixed films with better utilization of RuO_2.

Charge discharge study

Chronopotentiometry is used for the charge–discharge study of the samples (S1, S2, S3, and S4) from − 0.2 to +0.6 V vs. SCE at the current density of 1 mA/cm^2 in 0.5 M H_2SO_4 electrolyte as shown in Fig. 6.

The discharge profile usually contains two parts, first a resistive component arising from the sudden voltage drop representing the voltage change due to the internal resistance and a capacitive component related to changes in energy within the capacitor. An IR drop is observed in the each sample, which is attributed to the internal resistance of the electrode material. It is also observed that the IR drop is more for samples S1 (3:1) and S2 (1:1) and is decreased in samples S3 (1:3) and S4 (3:2). The large IR drop (421 mV) was observed for sample S1 (3:2). Moreover, comparatively less IR drop (91 mV) was observed for sample S3 (1:3) The sample S3 shows the good discharging behavior with large discharge time compared with other samples, which is responsible for its high specific energy. The values of specific power (SP) and specific energy (SE) are from earlier reported formulas [14]. The obtained values of the SE and SP are given in the Ragone plot as shown in Fig. 6a. The Ragone plot for mixed films shown in Fig. 6b shows that sample S3 (1:3) exhibits the specific power of 0.839 kW/kg and specific energy 11.18 Wh/kg. In addition, long cycle stability is vital parameter for the electrode material to apply effectively in supercapacitor. Therefore, the stability of the best sample (sample S3) was checked using cyclic voltammetry at higher scan rate of 100 mV/s over 2500 cycles. The stability curves for 1st and 2500th cycles are given in Fig. 7. It is observed that the CV curve shows the small variation even after 2500 cycles showing the good stability of the electrode material. The specific capacitance decreases from 45 to 39 F/g, which shows the 85% stability over the 2500 cycles.

Electrochemical impedance analysis

To investigate the electrochemical characteristics of the electrode and the electrolyte in quantitative manner impedance measurement is performed. The electrochemical impedance measurement (at open circuit voltage, in the frequency range of 10^5 to 10^{-2} Hz) of the SnO_2-RuO_2 mixed film for sample S3 (1:3) is carried out in 0.5 M H_2SO_4. The Nyquist depiction (Z' vs. Z'') of the raw impedance data for the sample S3 is shown in Fig. 8.

For the convenience of the interpretation, this plot can be divided into high- and low-frequency regions. The presence of semicircle in the high-frequency area suggests that there is a charge transfer resistance, while the straight line in the low-frequency region angled of the ~ 45° to the real axis is attributed to the capacitive behavior. Figure 8 shows the Nyquist plot for sample S3 as this sample showed good supercapacitive properties compared with other electrodes. A semicircle is observed at higher frequency region and straight line in low frequency region. In the Nyquist plot the value of semicircle corresponds to charge transfer resistance

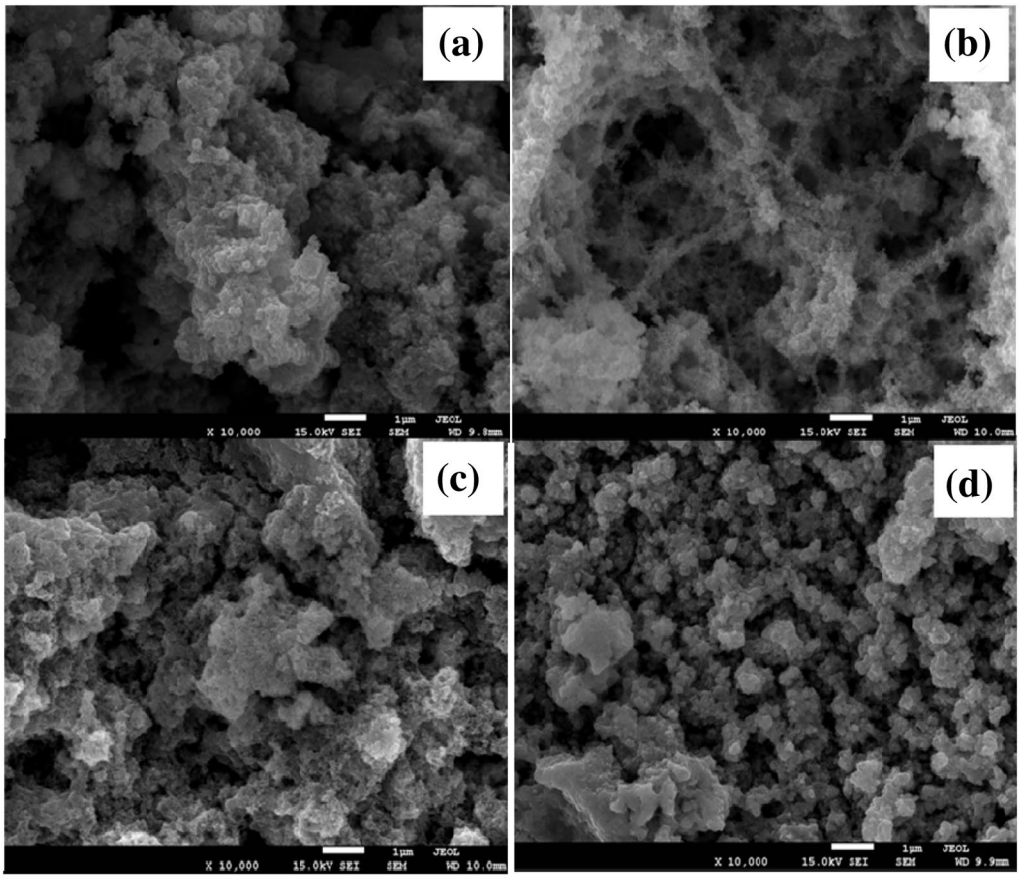
(a)
(b)
(c)
(d)
X 10,000 15.0kV SEI 1μm JEOL SEM WD 9.8mm
X 10,000 15.0kV SEI 1μm JEOL SEM WD 10.0mm
X 10,000 15.0kV SEI 1μm JEOL SEM WD 10.0mm
X 10,000 15.0kV SEI 1μm JEOL SEM WD 9.9mm

(e)

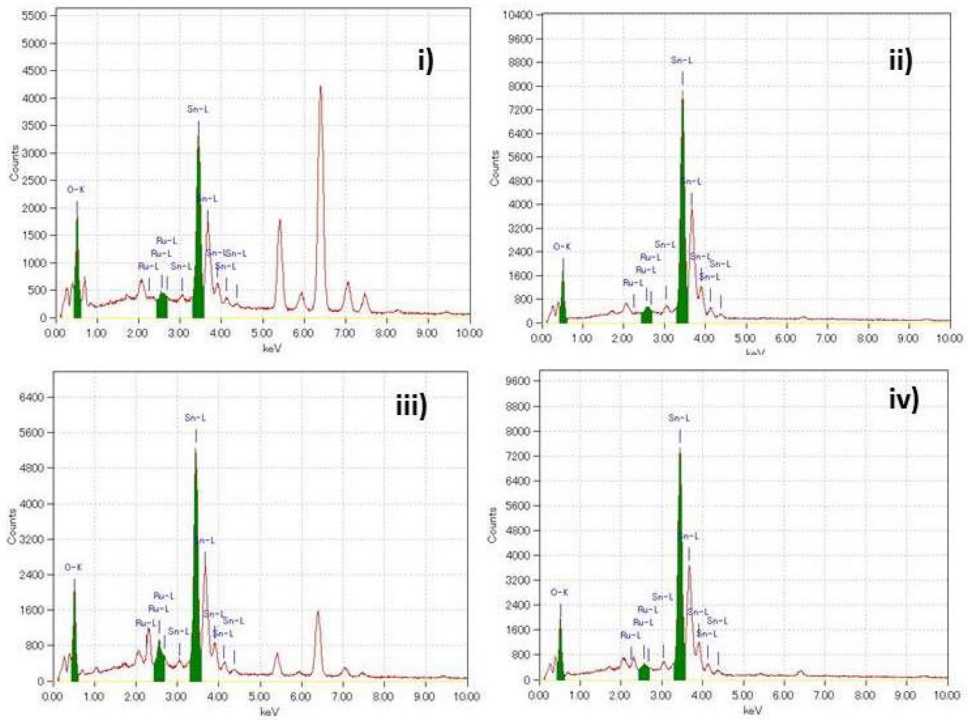
i)
ii)
iii)
iv)
Counts
keV
O-K
Ru-L
Sn-L

◂**Fig. 4** The SEM images of SnO_2-RuO_2 mixed films for samples (a) S1 (SnO_2:RuO_2, 3:2), (b) S2 (1:1), (c) S3 (1:3) and (d) S4 (2:3) at 10, 000X magnification, e) EDAX spectra for (i) S1 (SnO_2:RuO_2, 3:2), (ii) S2 (1:1), (ii) S3 (1:3) and (iv) S4 (2:3) samples deposited on stainless steel substrate

Table 2 SnO_2:RuO_2 cycle ratio in SILAR deposition

	S1 (3:2)	S2 (1:1)	S3 (1:3)	S4 (2:3)
Ru (at. %)	0.4	1.18	1.58	0.42
Sn (at. %)	13.93	23.17	16.33	22.41
O (at. %)	85.67	75.65	82.09	77.17

Compositions of Sn, Ru and O obtained from the EDAX analysis

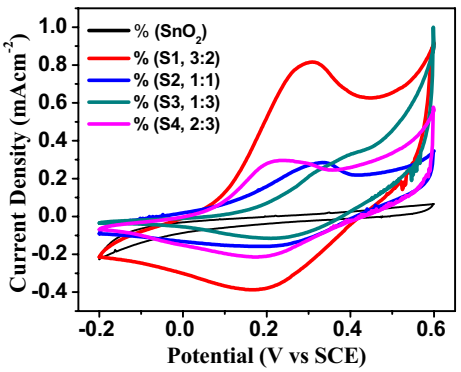

Fig. 5 The cyclic voltammograms of SnO_2-RuO_2 mixed films for samples (a) pure SnO_2, (b) S1 (SnO_2:RuO_2, 3:2), (c) S2 (1:1), (d) S3 (1:3) and (e) S4 (2:3) in the potential range of -0.2 to 0.6 V vs. SCE at the 5 mV.s^{-1} in 0.5 M H_2SO_4

Table 3 Effects of composition on the total specific capacitance ($C_{S,T}$) and specific capacitance based on RuO_2 ($C_{S,Ru}$) for SnO_2 combined with RuO_2 electrodes

Sample ID	$C_{S,T}$ (F.g^{-1})	$C_{S,Ru}$ (F.g^{-1})
S1 (3:2)	9	33
S2 (1:1)	25	137
S3 (1:3)	185	1010
S4 (2:3)	81	389

of the electrochemical reaction on the electrode surface. The values of charge transfer resistance for sample S3 are 24 Ω.

Bode representation of this data for sample S3 is shown in Fig. 9. The Bode plot at a phase angles of 34° and 82° reflects 82% and 23% of the power correspond to the heat production at the internal resistance. The loss factors of electrode 0.23 and 1.48 are calculated at a frequency 0.17 Hz and of 0.87 kHz, respectively, in the lower and higher frequency

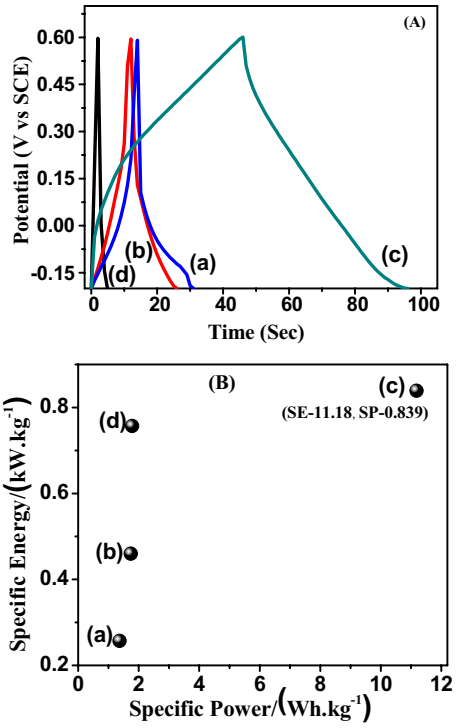

Fig. 6 **A**): The charge discharge curves of SnO_2-RuO_2 mixed films for samples (a) S1 (SnO_2:RuO_2, 3:2), (b) S2 (1:1), (c) S3 (1:3) and (d) S4 (2:3) in the potential window of − 0.2 to 0.6 V vs. SCE at the current density of 1 mA cm^{-2} in 0.5 M H_2SO_4. **B)** The Ragone plot for SnO_2-RuO_2 mixed films for samples (a) S1 (SnO_2:RuO_2, 3:2), (b) S2 (1:1), (c) S3 (1:3) and (d) S4 (2:3)

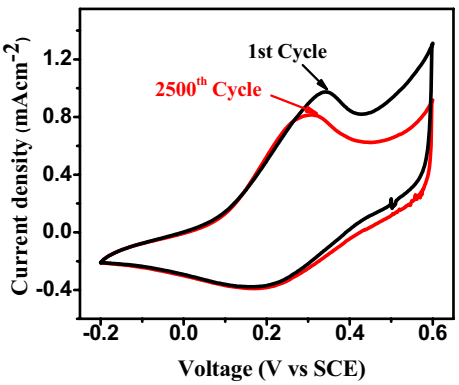

Fig. 7 The stability curve for Sample S3 at 100 mV/s scan rate in the potential window of − 0.2 to 0.6 V vs. SCE at the current density of 1 mA/cm^2 in 0.5 M H_2SO_4

region. The relaxation time constant (τ_0), calculated (plots of C'' (ω) vs. frequency) is shown in Fig. 10.

Relaxation time (τ_0) for the sample S3 is found to be 1.4 s. The τ_0 is a critical factor, which decides the applicability of electrode material according to energy demand. Small

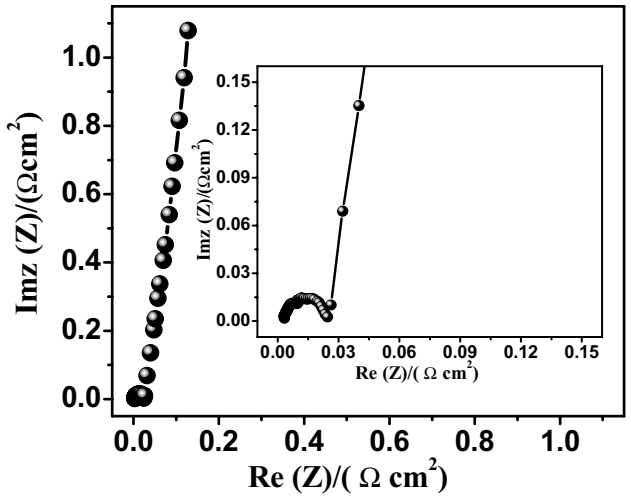

Fig. 8 Nyquist plot of SnO_2-RuO_2 mixed film, sample S3 (SnO_2:RuO_2, 1:3) in 0.5 M H_2SO_4

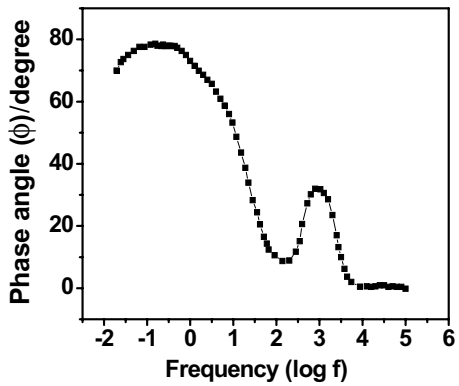

Fig. 9 Bode plot of SnO_2-RuO_2 mixed film, sample S3 (SnO_2:RuO_2, 1:3)

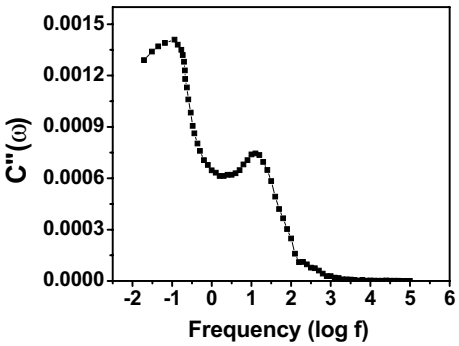

Fig. 10 Plot of imaginary capacitance (C'') vs. frequency for SnO_2-RuO_2 mixed film, sample S3 (SnO_2:RuO_2, 1:3)

relaxation time constant value exhibits a fast energy release capability of the electrode, to provide higher power density.

Conclusion

In conclusion, we have successfully synthesized SnO_2–RuO_2 mixed thin films by simple and inexpensive SILAR method at low temperature. Furthermore, the SnO_2 and RuO_2 content in the mixed thin films are varied by changing the deposition cycle, while making the mixed films. The structural results exhibit the transition from nanocrystalline mixed film to amorphous mixed films with increasing content of RuO_2. Likewise, the surface morphology changes from porous fibrous to porous framework of nanoparticles and finally agglomerated nanoparticles with increasing RuO_2 content. Finally, electrochemical performance of SnO_2-RuO_2 mixed thin films (1:3 ratio of SnO_2:RuO_2) shows the specific capacitance of 185 F/g with maximum utilization of RuO_2 with specific capacitance of 1010 F/g. Therefore, simple and inexpensive SILAR method can be used to enhance the electrochemical performance of other electrochemical materials by combining with precious and high electroactive RuO_2.

References

1. Kotz, R., Carlen, M.: Principles and applications of electrochemical capacitors. Electrochim. Acta **45**, 2483–2498 (2000)
2. Huggins, R.A.: Supercapacitors and electrochemical pulse sources. Solid State Ionics **134**, 179–195 (2000)
3. An, K.H., Kim, W.S., Park, Y.S., Moon, J.M., Bae, D.J., Lim, S.C., Lee, Y.S., Lee, Y.H.: Electrochemical properties of high-power supercapacitors using single-walled carbon nanotube electrodes. Adv. Funct. Mater. **11**, 387–392 (2001)
4. Conway, B.E.: Transition from "supercapacitor" to "battery" behavior in electrochemical energy storage. J. Electrochem. Soc. **138**, 1539–1548 (1991)
5. Zheng, J.P., Cygan, P.J., Jow, T.R.: Hydrous ruthenium oxide as an electrode material for electrochemical capacitors. J. Electrochem. Soc. **142**, 2699–2703 (1995)
6. Michell, D., Rand, D.A.J., Woods, R.: A study of ruthenium electrodes by cyclic voltammetry and X-ray emission spectroscopy. J. Electroanal. Interfacial Electrochem. **89**, 11–27 (1978)
7. Deshmukh, P.R., Pusawale, S.N., Jagdale, A.D., Lokhande, C.D.: Supercapacitive performance of hydrous ruthenium oxide (RuO_2·nH_2O) thin films deposited by SILAR method. J. Mater. Sci. **47**, 1533–1546 (2012)
8. Burke, L.D., Whelan, D.P.: The behaviour of ruthenium anodes in base. J. Electroanal. Interfacial Electrochem. **103**, 179–187 (1979)
9. Terrier, C., Chatelon, J.P., Roger, J.A.: Electrical and optical properties of Sb:SnO_2 thin films obtained by the sol-gel method. Thin Solid Films **295**, 95–100 (1997)
10. Hu, C.C., Wang, C.C., Chang, K.H.: A comparison study of the capacitive behavior for sol–gel-derived and co-annealed ruthenium–tin oxide composites. Electrochim. Acta **52**, 2691–2700 (2007)
11. Kim, H.K., Choi, S.H., Yoon, Y.S., Chang, S.Y., Ok, Y.W., Seong, T.Y.: Characteristics of RuO_2–SnO_2 nanocrystalline-embedded

amorphous electrode for thin film microsupercapacitors. Thin Solid Films **475**, 54–57 (2005)
12. Wang, C.C., Hu, C.C.: Electrochemical and textural characterization of binary Ru–Sn oxides synthesized under mild hydrothermal conditions for supercapacitors. Electrochim. Acta **50**, 2573–2581 (2005)
13. Wu, N.L., Kuo, S.L., Lee, M.H.: Preparation and optimization of RuO_2-impregnated SnO_2 xerogel supercapacitor. J. Power Sources **104**, 62–65 (2002)
14. Pusawale, S.N., Deshmukh, P.R., Gunjakar, J.L., Lokhande, C.D.: SnO_2–RuO_2 composite films by chemical deposition for supercapacitor application. Mater. Chem. Phys. **139**, 416–422 (2013)
15. Pathan, H.M., Lokhande, C.D.: Deposition of metal chalcogenide thin films by successive ionic layer adsorption and reaction (SILAR) method. Bull. Mater. Sci. **27**, 85–111 (2004)
16. Patake, V.D., Lokhande, C.D.: Chemical synthesis of nano-porous ruthenium oxide (RuO_2) thin films for supercapacitor application. Appl. Surf. Sci. **254**, 2820–2824 (2008)
17. Lee, W., Mane, R.S., Todkar, V.V., Lee, S., Egorova, O., Chae, W.S., Han, S.H.: Implication of liquid-phase deposited amorphous RuO_2 electrode for electrochemical supercapacitor. Electrochem. Sol. State Lett. **10**, A225–A227 (2007)
18. Yu, K.N., Xiong, Y., Liu, Y., Xiong, C.: Microstructural change of nano-SnO_2 grain assemblages with the annealing temperature. Phys. Rev. B **55**, 2666–2671 (1997)
19. Bhaskar, S., Dobal, P.S., Majumder, S.B., Katiyar, R.S.: X-ray photoelectron spectroscopy and micro-Raman analysis of conductive RuO_2 thin films. J. Appl. Phys. **89**, 2987–2991 (2001)
20. Ryan, J.V., Berry, A.D., Anderson, M.L., Long, J.W., Stroud, R.M., Cepak, V.M., Browning, V.M., Rolison, D.R., Merzbacher, C.I.: Electronic connection to the interior of a mesoporous insulator with nanowires of crystalline RuO_2. Nature **406**, 169–172 (2000)
21. Hu, C.C., Chang, K.H., Wang, C.C.: Two-step hydrothermal synthesis of Ru–Sn oxide composites for electrochemical supercapacitors. Electrochim. Acta **52**, 4411–4418 (2007)
22. Hu, C.C., Chen, W.C., Chang, K.H.: How to Achieve Maximum Utilization of Hydrous Ruthenium Oxide for Supercapacitors. J. Electrochem. Soc. **151**, A281–A290 (2004)
23. Hu, C.C., Chen, W.C.: Effects of substrates on the capacitive performance of $RuOx{\cdot}nH_2O$ and activated carbon–RuOx electrodes for supercapacitors. Electrochim. Acta **49**, 3469–3477 (2004)
24. Chang, K.-H., Hu, C.-C.: Oxidative synthesis of $RuOx \cdot n\ H_2O$ with ideal capacitive characteristics for supercapacitors. J. Electrochem. Soc. **151**, A958–A964 (2004)